NON-ISOTHERMAL MODELING AND SIMULATION FOR A SOLUBLE-LEAD ACID FLOW BATTERY

Amir A-K. Omran, Hassan. Al-Fetlawi, Falah K. Matlub
Department of Electrochemical Engineering,
Babylon University, Hilla City, Iraq

ABSTRACT
Non-isothermal two-dimensional transient model for a soluble lead-acid flow battery is developed, including the negative electrode, positive electrode and the flow space between them. The model based on a comprehensive description of mass, charge, energy and momentum transport and conservation, and is combined with a global kinetic model for reactions involving lead species. The influence of the applied current density, operating temperature, inlet electrolyte velocity and initial concentration of lead ions on the charge/discharge behavior are investigated. Numerical simulations have shown increasing the applied current density can decrease the cell voltage. Increasing cell temperature improved the cell voltage with a very little effect on the outlet concentrations, so cell temperature can be considered a key parameter to optimize the performance. Simulated behavior shows a very little effect with variations in the inlet electrolyte velocity, while changing in the initial concentration of lead ions have shown a good influence on the performance.

KEY WORDS: *Redox flow batteries, soluble lead-acid, non-isothermal, modeling, simulation.*

I. INTRODUCTION

Among rechargeable batteries, the redox flow batteries (RFB) have some advantages where the electrodes are not being part of electrochemical fuel. The electrodes do not undergo physical and chemical changes during operation, thus leading to more stable and durable performance [1]. Long charge/discharge cycle service life is realized. The storage capacity can be increased easily by increasing the capacity of the electrolyte tanks (installing additional tanks) [2]. Energy storage capability depends on the quantity of the reactant species in solution [3]. Scale up can be easily achieved by increasing the electrode size or by adding more electrodes in each stack. Power can be simply determined by the numbers of cells in the stack and size of electrodes. The applications of redox flow batteries are numerous, including load leveling and peak shaving, power quality control application, facilitating renewable energy deployment and energy storage for electric vehicles [4, 5].
The soluble lead-acid redox flow battery proposed over the last ten years by Pletcher and *et al* has two inert electrodes and a single electrolyte of lead methanesulfonate, $Pb(CH_3SO_3)_2$, in methanesulfonic acid, (CH_3SO_3H), and it is based on the electrode reactions of Pb(II) in the acid [6, 7]. During charge, lead deposits at the negative electrode while lead dioxide deposits at the positive one. While During discharge, the lead and lead dioxide layers re-dissolve via oxidation and reduction, respectively, back to the soluble lead(II) ion [6, 8].

$$Pb \rightleftharpoons Pb^{2+} + 2e^- \quad (1)$$

$$PbO_2 + 4H^+ + 2e^- \rightleftharpoons Pb^{2+} + 2H_2O \quad (2)$$

The overall cell reaction is:

$$Pb + PbO_2 + 4H^+ \rightleftharpoons 2Pb^{2+} + 2H_2O \quad (3)$$

The lead acid flow system differs from the traditional lead acid battery [9] since the electrolyte is aqueous methanesulfonic acid and lead ions is highly soluble in this acid [10]. While the very familiar static lead acid battery operates with a sulfuric acid electrolyte where the source of the Pb(II) is an insoluble lead sulfate present in a paste on the surface of the two electrodes [11, 12]. In comparison

with other flow batteries, the soluble lead acid flow battery has the key advantage that it employs only a single electrolyte and therefore operates without a membrane separator [7]. This simplifies the cell design and halves the number of pumps and reservoirs in the system, as well as avoiding the cost problems associating with membrane [7, 9]. The absence of a membrane also has appositive influence on the energy efficiency and the cell chemistry avoids the problems associated with leakage and cross-contamination of species through a membrane that severely hampered other flow batteries [6].
The approaching commercialization of a whole class of redox flow cell storage systems sets a series of new challenges to developers of this new technology, notably scale-up and optimization (with regards to flow geometries and operating conditions), improvement in electrolyte stability, development of electrode materials resistant to oxidation. Many of these challenges are not particularly well suited to laboratory analysis alone, by virtue of the associated financial costs and long timescales. In such cases it is beneficial to employ modeling and simulation as a means of down-selecting laboratory test scenarios so that, wherever possible, extensive laboratory experimentation can be avoided.
This work has done at the Electrochemical Engineering Department at the University of Babylon.

II. MODEL DEVELOPMENT

2.1 Model assumptions

The model is based on the two-dimensional slice depicted in Figure 1. The two-dimensional approximation leads to a considerable saving in computational time without a major loss in accuracy if the electrolyte flow rate is reasonably high, as in normal operation. The reactions that occur in the soluble lead acid flow battery during charge and discharge have shown by reaction (1) and (2).

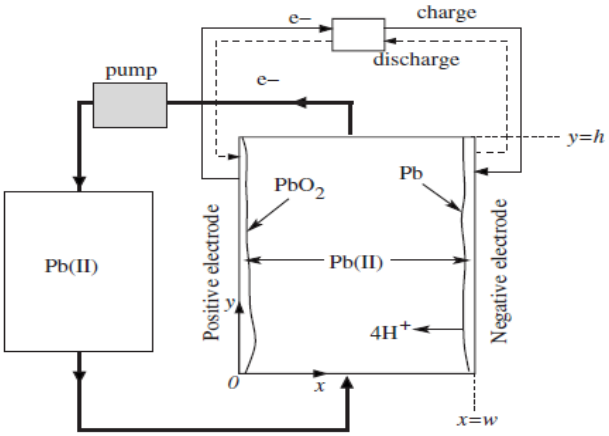

Figure 1: The soluble lead acid battery and the flow system.

The following assumptions have been made in the present study:
The dilute solution approximation is employed, assuming water to be a dominant component, so water properties for density and viscosity are used. Flow is considered laminar and incompressible. Side reactions involving PbO_x formation reaction and oxygen evolution reaction are not considered. The thicknesses of the Pb and PbO_2 deposits are small compared to the reactor dimensions and are, therefore, neglected. The electrolyte mixture only dissociate into Pb^{2+}, H^+, and HSO_4^-.

2.2 Model equations

2.2.1 Principles of conservation

A volume-averaged mass balance for each species (Pb^{2+}, H_2O and H^+) in the liquid electrolyte can be expressed in the following form:

$$\frac{\partial c_i}{\partial t} + \nabla N_i = -S_i \qquad (3)$$

S_i is the source term for species i, the source term defined in Table 1.

Table 1: Source and sinks for the liquid phase for equation (3).

Source term	-ve electrode	+ve electrode
Pb^{2+}	$\nabla.\vec{i_1}/2F$	$\nabla.\vec{i_2}/2F$
H_2O	–	$\nabla.\vec{i_2}/F$
H^+	–	$2\,\nabla.\vec{i_2}/F$

For concentration fluxes, modified Nernst-Planck can be used, in which transport of a charged species occur by diffusion, migration, and convection. The total flux is:

$$\vec{N_i} = -D_i\,\nabla c_i - \frac{z_i c_i D_i}{RT} F\,\nabla\phi_e + \vec{u}c_i \tag{4}$$

The electrolyte is considered to be electrically neutral, $\sum_i z_i c_i = 0$

The bulk flow velocity of the electrolyte solution is given by the incompressible Navier–Stokes equation and continuity equations.

$$\rho\frac{\partial\vec{u}}{\partial t} + \rho\,(\vec{u}.\nabla)\vec{u} = -\nabla p + \mu\,\nabla^2\vec{u} \tag{5}$$

$$\nabla\,\vec{u} = 0 \tag{6}$$

The total current density in the electrolyte can be calculated, using electroneutrality condition:

$$\vec{i_e} = \sum_i z_i F\,\vec{N_i} = -\sigma_e\,\nabla\phi_e - F\sum_i z_i D_i\,\nabla c_i \tag{7}$$

where the ionic conductivity, σ_e, is given by:

$$\sigma_e = \frac{F^2}{RT}\sum_i {z_i}^2\,D_i c_i \tag{8}$$

At all points, including the boundaries, the ionic and electronic currents satisfy the condition of charge conservation yields:

$$\nabla.\vec{i_e} + \nabla.\vec{i_s} = 0 \tag{9}$$

The electronic potential in the electrodes is given by Ohm's law:

$$-\sigma_s\,\nabla^2\phi_s = -\nabla.\vec{i} \tag{10}$$

2.2.2 Reaction kinetics and cell voltage

From the Butler–Volmer expression for charge-transfer kinetics. The common approximation of equal charge-transfer coefficients for the forward and reverse reactions has been made for the reactions at both electrodes

$$i_1 = Fk_0^{Pb}c_{Pb^{2+}}\left[exp\left(\frac{F\,\eta_-}{RT}\right) - exp\left(\frac{F\,\eta_-}{RT}\right)\right] \tag{11}$$

$$i_2 = Fk_0^{PbO_2}\,c_{Pb^{2+}}\left(\frac{c_{H^+}}{c_{H^+}^0}\right)\left[exp\left(\frac{F\,\eta_+}{RT}\right) - exp\left(\frac{F\,\eta_+}{RT}\right)\right] \tag{12}$$

where the overpotential is given by:

$$\eta_\pm = \phi_{s_\pm} - \phi_e - E_\pm \tag{13}$$

where $E_\pm$ are the open-circuit potentials for reaction (1) and (2), respectively, estimated from the Nernst equations:

$$E_- = E_{0,1} + \frac{2.3RT}{F}\ln c_{Pb^{2+}} \tag{14}$$

$$E_+ = E_{0,2} + \frac{2.3RT}{F}(\ln c_{Pb^{2+}} - \ln c_{H^+}) \tag{15}$$

2.2.3 Energy balance

The energy balance takes into account heat conduction, convective heat transport and heat generation by reaction and ohmic resistance. As a reasonable first approximation it is assumed that the liquid and solid phases in the same temperature. The energy balance is thus:

$$\frac{\partial}{\partial t}(\overline{\rho_l C_l}T) + \nabla.(\vec{u}\rho_l C_l T) - \bar{\lambda}\nabla^2 T = \sum_k Q_k \tag{16}$$

The heat generation term, Q_k are defined in Table 2: they represent heating by activation losses, reaction and ohmic resistance.

Table 2: Sources and sinks for the energy equation (18).

Term	-ve electrode	+ve electrode
Q_{act}	$\eta_1 \nabla.\overrightarrow{i_1}$	$\eta_2 \nabla.\overrightarrow{i_2}$
Q_{rev}	$-\Delta S_1 T \nabla.\overrightarrow{i_1}/F$	$-\Delta S_2 T \nabla.\overrightarrow{i_2}/F$
Q_{ohm}	$\sigma_s \lvert\nabla\phi_s\rvert^2 + \sigma_e \lvert\nabla\phi_e\rvert^2$	$\sigma_s \lvert\nabla\phi_s\rvert^2 + \sigma_e \lvert\nabla\phi_e\rvert^2$

These standard reaction entropies are given by:

$$\Delta S_{0,j} = \left(\sum_{products} S_{0,j}^{products}\right) - \left(\sum_{reactants} S_{0,j}^{reactants}\right) \quad (17)$$

where $S_{0,j}^{products}$, $S_{0,j}^{reactants}$ are the standard entropies of formation of the products and reactants in reactions (j = 1, and 2). Their values at 298.15 K. For each reaction j, the standard reaction entropy is related to the standard Gibbs free energy change of the reaction,$\Delta G_{0,j}$, and the standard enthalpy change of reaction, $\Delta H_{0,j}$, by the thermodynamic relation:

$$\Delta G_{0,j} = \Delta H_{0,j} - T\Delta S_{0,j} \quad (18)$$

Using equation (18) and the relation $\Delta G_{0,j} = -nFE_{0,j}$, where $E_{0,j}$ is the standard potential of reaction j, the temperature dependence of $\Delta S_{0,j}$ is obtained:

$$-nF\frac{\partial \Delta E_{0,j}}{\partial T} = \frac{\partial \Delta G_{0,j}}{\partial T} = \Delta S_{0,j} \quad (19)$$

The standard potentials $E_{0,1}$, $E_{0,2}$ are functions of temperature [13]:

$$E_0^T = E_0^{298} + (T - 298)\left(\frac{dE_0}{dT}\right)_{298} \quad (20)$$

where E_0^{298} is the standard electrode potential at T= 298 K , $\left(\frac{dE_0}{dT}\right)_{298}$ is the temperature coefficient of the standard electrode potential. So the standard electrode potentials at both the negative and positive electrodes, respectively are:

$$E_{0,1}^T = E_{0,1}^{298} + (T - 298)(-395 \times 10^{-5}) \quad (21)$$

$$E_{0,2}^T = E_{0,2}^{298} + (T - 298)(-253 \times 10^{-5}) \quad (22)$$

The reaction constants are also temperature dependent. They can be written in Arrhenius form as follows [14]:

$$k_j = k_{ref,j} \exp\left(-\frac{\Delta G_{0,j}}{R}\left[\frac{1}{T_{ref,j}} - \frac{1}{T}\right]\right) \quad (23)$$

and hence;

$$k_j = k_{ref,j} \exp\left(\frac{nFE_{0,j}}{R}\left[\frac{1}{T_{ref,j}} - \frac{1}{T}\right]\right) \quad (24)$$

where $k_{ref,j}$ is the values of k_j at a reference temperature $T_{ref,j}$ (j = 1, 2).

2.2.4 Reservoir and recirculation equations

The movement of the electrolyte solution between the electrodes and the pump alters the concentrations at the inlet boundaries with time. Invoking conservation of volume, the volumetric flow at the outlet boundary, which has a cross-sectional area A_{out}, is $\omega = v_{in}A_{out}$. From the calculated average concentration at the outflow boundary,

$$c_i^{out} = \int_{y=h} c_i \, dx \quad (25)$$

The inlet concentrations are approximated from the following mass balance, which assumes instantaneous mixing and negligible reaction in the reservoir of electrolyte volume, V.

$$\frac{dc_i^{in}}{dt} = \frac{\omega}{V}\left(c_i^{out} - c_i^{in}\right); \quad c_i^{in}(0) = c_i^0 \quad (26)$$

The inlet temperature is determined by a heat balance performed along similar lines (assuming that density and specific heat capacity of the solutions are constant and that instantaneous mixing occurs in the reservoirs):

$$\frac{dT^{in}}{dt} = \frac{\omega}{V}\left(T^{out} - T^{in}\right); \quad T^{in}(0) = T_0 \quad (27)$$

where T^{in} and T^{out} are the temperatures at the inflow and outflow boundaries, respectively.

2.3 Initial and boundary conditions

Along the electrode surfaces, a Neumann condition was applied for the pressure:

$$\nabla p.\vec{n} = 0 \qquad \text{(Except inlet and outlet surfaces)} \qquad (28)$$

At the inlet, each species of the liquid electrolyte solution enters with a prescribed bulk velocity and the species concentrations are given:

$$c_i = c_i^{in}(t) \qquad \text{and } \vec{u} = (0, v_{in}) \qquad \text{(inlets)} \qquad (29)$$

At the outlets, the liquid pressure is prescribed and the diffusive fluxes of the species are set to a zero value (fully developed flow conditions):

$$-D_i \nabla c_i .\vec{n} = 0 \qquad p = p_{out} \qquad \text{(outlets)} \qquad (30)$$

At the electrode surfaces, no-slip conditions are applied:

$$\vec{u} = 0; \qquad x = 0,\ x = w \qquad (31)$$

The flux conditions for the potential distribution of the electrodes are as follow:

$$-\sigma_s \nabla\phi_s = 0; \qquad x = 0,\ x = w,\ y = 0,\ y = h \qquad (32)$$

The potential distribution for electrolyte is specified as (during charge):

$$-\sigma_e \nabla\phi_e.\vec{n} = \begin{cases} I_{app}; & x = 0 \\ -I_{app}; & x = w \end{cases} \qquad (33)$$

For the discharge signs are reversed.

The temperature at the inlets is given separately as:

$$T = T^{in} \qquad (34)$$

Consistent initial conditions are prescribed for the concentrations and potentials, as follows:
At the negative electrode:

$$\begin{gathered} c_i = c_i^0 \\ \phi_{s\_} = E_- \\ \phi = 0 \end{gathered} \qquad (35)$$

At the positive electrode:

$$\begin{gathered} c_i = c_i^0 \\ \phi_{s+} = E_+ \\ \phi = 0 \end{gathered} \qquad (36)$$

The initial temperature is uniform through the cell:

$$T(t = 0) = T_0 \qquad (37)$$

2.4 Numerical details

The model presented above was solved using the COMSOL Multiphysics® package, with a combination of the convection–diffusion, general-form and PDE options. The package is based on the finite-element method; a quadratic basis was used in all of the simulations, together with 13528 elements. The relative error tolerance was set to 1×10^{-6}. The default set of operating conditions is given in Table 4 and the default parameter values are given in Tables (3, 5, 6, 7).

III. RESULTS AND DISCUSSION

3.1 Effect of the applied current

Figure 2 shows simulated charge-discharge curves at different applied current densities: i_{app} = 5 mA cm^{-2}, 10 mA cm^{-2}, 20 mA cm^{-2}, 30 mA cm^{-2} and 40 mA cm^{-2}. The sign of the current is reversed during discharge. In all cases the initial temperature is T_0 = 298 K, the Pb(II) initial concentration is 700 mol m^{-3} and the inlet electrolyte velocity is 10 cm s^{-1}. As the applied current density is increased, the cell voltage increases during charge, and the drop in cell voltage between charge and discharge increases. This is primarily due to the increased ohmic resistance as the current density increased. The

effect of applied current density on the Pb(II) reactant concentration is demonstrated in Figure 3 with positive electrode placed at x = 0 and the negative electrode at 3.5 mm , which shows concentration profiles of Pb(II), for (a) an applied current density of 20 mA cm^{-2} and (b) an applied current density of 40 mA cm^{-2} with v_{in} = 10 cm s^{-1} and Pb(II) initial concentration of 700 mol m^{-3} in both cases. Comparing Figure 3(a) and (b) reveals that the Pb(II) is more uniform at the lower current density, a direct consequence of the slower rates of reaction at surfaces.

Figure 4 shows the evolution of the lead ions concentration at the intersection between the outlet and the positive electrode, y = 2 cm and x = 0 mm for the two cases of applied current densities, i_{app}= 20 mA cm^{-2} and i_{app}= 40 mA cm^{-2}. Where the low applied current densities (i.e. i_{app}= 5 mA cm^{-2}, i_{app}= 10 mA cm^{-2} and 30 mA cm^{-2}) have shown a similar effect as i_{app}= 20 mA cm^{-2}. It is clear that at lower current densities the Pb(II) depletion during charge is less than the depletion at higher current densities. In the case of i_{app}= 20 mA cm^{-2} Pb(II) outlet concentration reached a value of 690 mol m^{-3} at the end of the charge phase, while the concentration reached a value of 686 mol m^{-3} in the case of i_{app}= 20 mA cm^{-2}. At the end of the discharge phase the outlet concentration was 699 mol m^{-3} with low current densities and it was 698 mol m^{-3} with higher current density. This is mainly due to the increasing in the overvoltage especially the ohmic one which lead to loss the Pb(II) concentration and not being back to the initial concentration 700 mol m^{-3} when the cell is discharged.

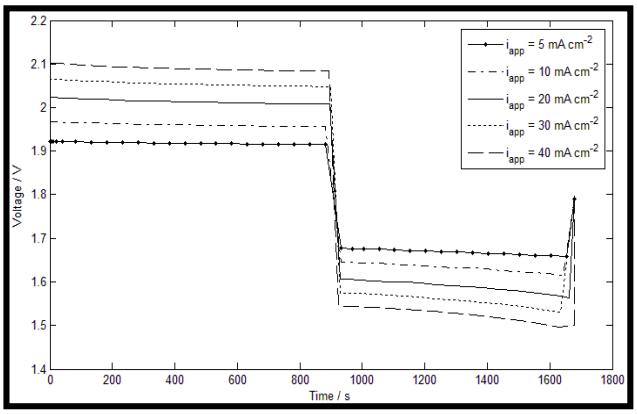

Figure 2: Simulated charge/discharge curves at different values of applied current densities: i_{app} = 5 mA cm^{-2}, 10 mA cm^{-2}, 20 mA cm^{-2}, 30 mA cm^{-2} and 40 mA cm^{-2}. The operating temperature is 298K, the Pb(II) initial concentration is 700 mol m^{-3} and the inlet electrolyte velocity is 10 cm s^{-1}.

(a)

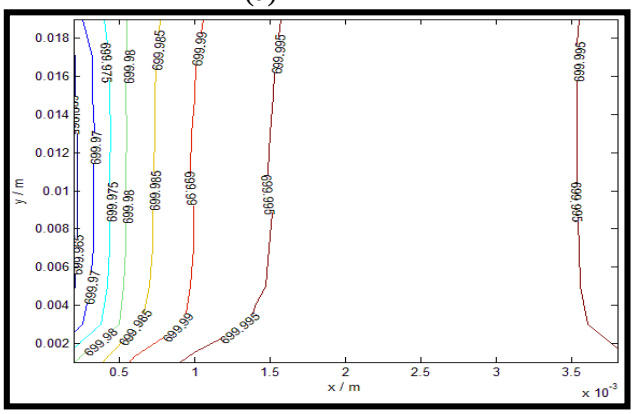

Figure 3a: Contours of Pb(II) concentration profiles in (mol/m^3) for i_{app} = 20 mA cm^{-2} at a temperature of 298 K, Pb(II) initial concentration of 700 mol m^{-3} and inlet electrolyte velocity of 10 cm s^{-1}.

(b)

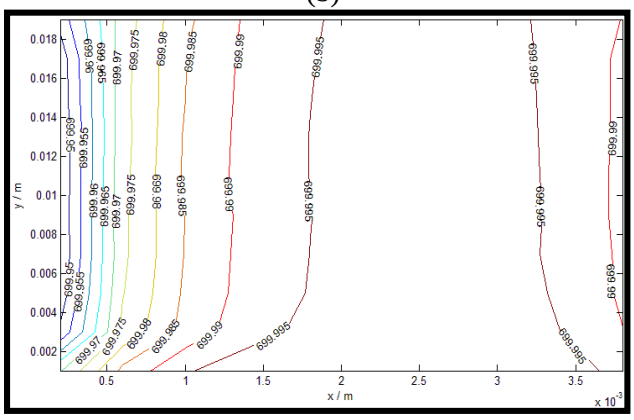

Figure 3b: Contours of Pb(II) concentration profiles in (mol m^{-3}) for i_{app} = 40 mA cm^{-2} at a temperature of 298 K, Pb(II) initial concentration of 700 mol m^{-3} and inlet electrolyte velocity of 10 cm s^{-1}.

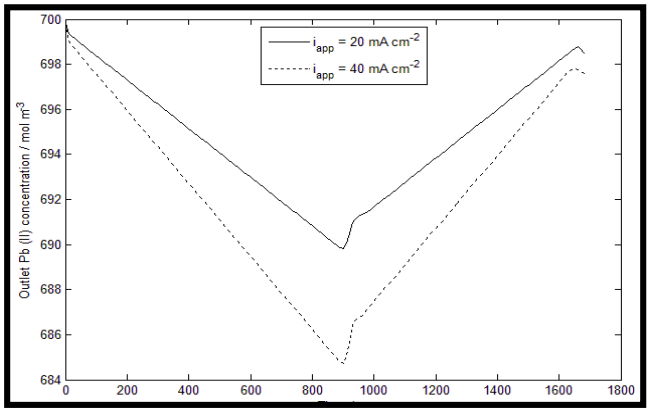

Figure 4: The evolution of Pb(II) concentration at the intersection between the outlet and the positive electrode, y = 2 cm and x = 0 mm for i_{app} = 20 mA cm^{-2} and i_{app} = 40 mA cm^{-2}. At a temperature of 298 K, Pb(II) initial concentration of 700 mol m^{-3} and inlet electrolyte velocity of 10 cm s^{-1}.

3.2 Effect of the operating temperature

Figure 5 shows the evolutions of the cell voltage during a charge/discharge cycle at different operating temperatures, T_0 = 273 K, 298 K, 313 K, 323 K and 333 K. The applied current density is 20 mA cm^{-2}, the Pb(II) initial concentration is 700 mol m^{-3} and the inlet electrolyte velocity is 10 cm s^{-1}. In all cases the system is assumed to be adiabatic.

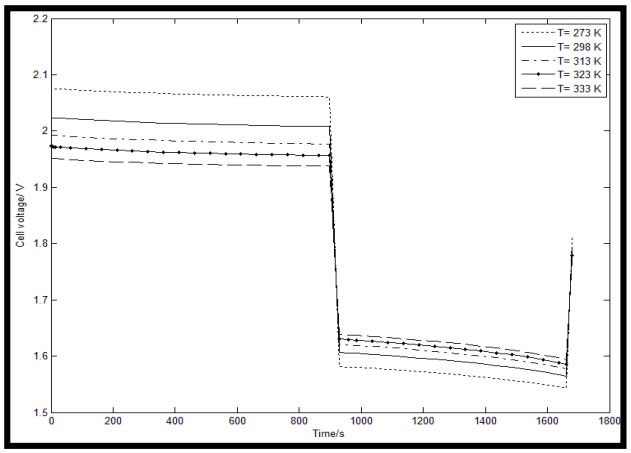

Figure 5: Simulated charge/discharge curves at different operating temperatures T_0 = 273 K, 298 K, 313 K, 323 K and 333 K. The times to charge and discharge are approximately 900 s and 1680 s in each case, respectively. The Pb(II) initial conc. is 700 mol m^{-3}, i_{app} is 20 mA cm^{-2} and v_{in} is 10 cm s^{-1}.

During charge, there is a clear decrease in the cell voltage as the temperature is raised and during discharge the cell voltage is increased, i.e., the deviation of the cell voltage from the equilibrium value decreases as the temperature is increased, this behavior is in agreement with published work by Al-Fetlawi and *et al* [18], but Alex Bates and *et al* [16] have showed opposite behavior with increasing temperature. The decreasing deviation of the cell voltage from the equilibrium value with increasing temperature is due to reduction in the equilibrium potentials given by equations (14) and (15) and equations (21) and (22) for fixed initial concentrations of the reactants and also increasing the rate constants, k_j, given in equations (23) and (24). For lower temperatures, the decreased reaction rate constant leads to an increase in the magnitude of the overpotential, as seen from the Butler-Volmer equations (11) and (12).

3.3 Effect of the inlet electrolyte velocity

Simulation results have shown that the variations in the inlet electrolyte velocity have very little effect on cell voltage during charge and discharge. Increasing the inlet electrolyte velocity in the range $(2 - 20)$ cm s^{-1} lead to change in the charge/discharge voltages in the range of about 0.01 V. Figure 6 compares the charge/discharge curves for the base case v_{in} = 10 cm s^{-1} with v_{in} = 2 cm s^{-1}, 5 cm s^{-1}, 15 cm s^{-1} and 20 cm s^{-1}.

Only when the inlet electrolyte velocity varies from 10 cm s^{-1} to 20 cm s^{-1}, there was a change in the concentration of Pb(II) with time in the intersection point between the outlet ant the positive electrode, y = 2 cm and x = 0 mm. At the end of the charge phase the concentration reached 690 mol m^{-3} with v_{in} = 10 cm s^{-1} and reached 691 mol m^{-3} with v_{in} = 20 cm s^{-1}. In the end of the discharge the effect also was little, that Pb(II) concentration changed from 699 mol m^{-3} to 698 mol m^{-3} as shown in Figure 7. The inlet electrolyte velocity primarily affects the convection flux of species.

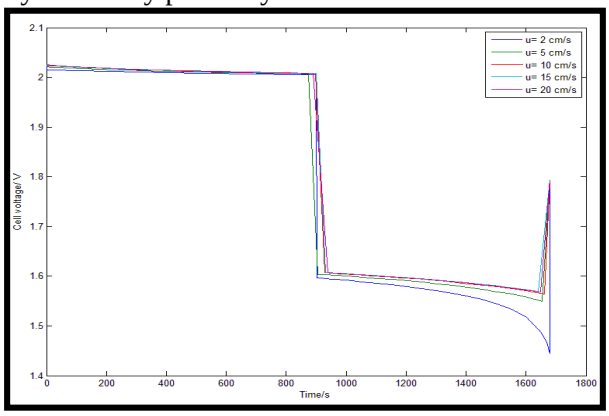

Figure 6: Simulated charge-discharge curves at different inlet electrolyte velocities; v_{in} = 2 cm s^{-1}, 5 cm s^{-1}, 10 cm s^{-1}, 15 cm s^{-1} and 20 cm s^{-1}. The i_{app} = 20 mA cm^{-2}, the initial Pb(II) conce. = 700 mol m^{-3} and the T = 298 K.

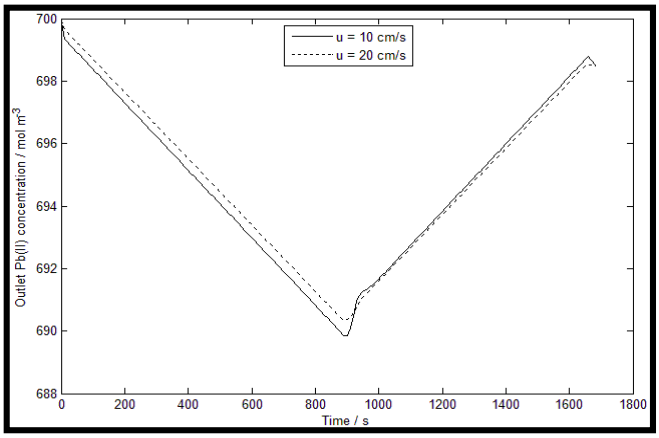

Figure 7: The evolution of Pb(II) concentration at the intersection between the outlet and the positive electrode, y = 2 cm and x = 0 mm at v_{in} = 10 cm s^{-1} and v_{in} = 20 cm s^{-1}, with i_{app} = 20 mA cm^{-2}, the initial Pb(II) conce. = 700 mol m^{-3} and T =298 K for both cases.

3.4 Effect of the Pb(II) initial concentration

Figure 8 shows the changes in the simulation charge/discharge voltages versus time resulting from changes in the initial concentration of Pb(II). Increasing the Pb(II) initial concentration in the electrolyte reduces the voltage during charge, voltage is only slightly affected during discharge.

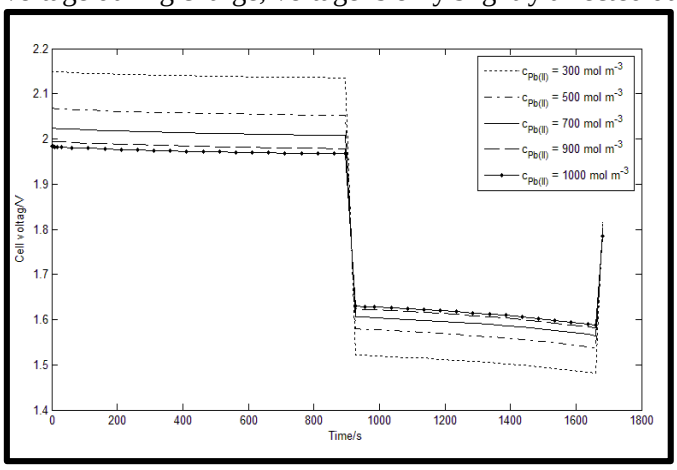

Figure 8: Simulated charge/discharge curves at different initial concentration of Pb(II); 300 mol m^{-3}, 500 mol m^{-3}, 700 mol m^{-3}, 900 mol m^{-3} and 1000 mol m^{-3}, at T = 298 K, iapp = 20 mA cm^{-2} and v_{in} = 10 cm s^{-1}.

IV. CONCLUSIONS

A non-isothermal transient two-dimensional model for the soluble lead-acid redox flow battery has been developed. The impact of changing the operating conditions, including applied current density, temperature, inlet electrolyte velocity, and Pb(II) initial concentration on the performance was investigated.

Increasing the applied current density badly affected the performance. Voltage efficiency markedly decreased with higher current densities due to the high overpotential associated with high current densities. Also increasing the applied current density has increased the depletion rate of Pb(II) during charge and lower the outlet Pb(II) concentration.

Higher operating temperatures enhanced the performance by reducing the overpotentials, increasing the reaction rate and improving the voltage efficiency. This indicates cell temperature may be a key in optimizing a lead acid flow battery.

Changing the inlet electrolyte velocity showed no significant effect on the cell voltage and little effect on the voltage efficiency. But, the outlet Pb(II) concentration increased during charge and decreased during discharge with increasing the inlet electrolyte velocity.

Increasing the initial concentration of Pb(II) reduces the cell voltage during charge and slightly increases it during discharge. While, the voltage efficiency increased with changing the Pb(II) initial concentration.

V. RECOMMENDATIONS FOR FUTURE WORK

The framework developed can be extended to other flow battery systems with some modifications. Some specific extensions can be included to the present work are: effect of oxygen evolution reaction; it is a competing reaction may occur on the positive electrode during charge exhausting some of the applied energy and leading to deterioration in the performance and effect of PbO formation reaction; this component is a side product formed on the positive electrode during discharge leading to loss in the active species (i.e. Pb(II)) and loss in battery performance.

Table 3: Default values of the constants related to the structure.

Symbol	Quantity	Value
h	Electrode height	0.02 m
w	Electrode separation	0.004 m
d	Electrode thickness	0.01 m

$A_{in/out}$	Inlet/Outlet cross section area	4×10^{-5} m^2
V	Reservoir volume	3.92×10^{-5} m^3
A_s	Active electrode surface area	2×10^{-4} m^2

Table 4: Default initial and boundary values.

Symbol	Quantity	Value
T_{ref}	Reference temperature	298 K
$c^0_{Pb(II)}$	Initial lead ion concentration	700 mol m^{-3}
c^0_{H+}	Initial proton concentration	50 mol m^{-3}
$c^0_{H_2O}$	Initial water concentration	4700 mol m^{-3}
p_{out}	Negative electrode outlet pressure	300 K Pa [15]
v_{in}	Inlet electrolyte velocity	0.1 m s^{-1}
i_{app}	Applied current density	200 A m^{-2} [15]

Table 5: Default values of the constants related to electrochemistry.

Symbol	Quantity	Value
$k_{ref,1}$	Standard rate constant for reaction 1	2.1×10^{-7} m s^{-1} [15]
$k_{ref,2}$	Standard rate constant for reaction 1	2.5×10^{-7} m s^{-1} [15]
E^0_+	Positive electrode standard potential	1.458 V [13]
E^0_-	Negative electrode standard potential	−0.395 V [13]

Table 6: Default values for constants related to the transport of charge and mass.

Symbol	Quantity	Value
$D_{Pb(II)}$	Pb(II) diffusion coefficient in electrolyte	2.4×10^{-10} m^2 s^{-1} [15]
D_{H^+}	H^+ diffusion coefficient in electrolyte	1.4×10^{-9} m^2 s^{-1} [15]
D_{H_2O}	H_2O diffusion coefficient in electrolyte	2.3×10^{-9} m^2 s^{-1} [15]
$D_{HSO_4^-}$	HSO_4^- diffusion coefficient in electrolyte	1.23×10^{-9} m^2 s^{-1} [15]
μ_{H_2O}	Water viscosity	10^{-3} Pa. s [15]

Table 7: Default parameter values for the heat equation and thermodynamic values of the aqueous species at 25°c.

Symbol	Quantity	Value
λ	Electrolyte thermal conductivity	0.6 W m^{-1} K^{-1}
$\rho_l C_l$	Liquid thermal capacitance (water)	4.187×10^6 J m^{-2} K^{-1}
$-\Delta S_1$	Entropy associated with reaction 1	43.59 J mol^{-1} K^{-1} [17]
$-\Delta S_2$	Entropy associated with reaction 2	-84.73 J mol^{-1} K^{-1} [17]
$-\Delta H_1$	Enthalpy associated with reaction 1	-1632.85 J mol^{-1} [17]
$-\Delta H_2$	Enthalpy associated with reaction 2	293598.53 J mol^{-1} [17]

Nomenclature

Roman Symbol	**Definition**	**Unit**
A	Area	m^2
C	Specific heat capacitance	J Kg^{-1} K^{-1}
c	Concentration	mol m^{-3}
D	Diffusion coefficient	m^2 s^{-1}
d	Thickness	m
E	Potential	V
F	Faraday's constant	C mol^{-1}
h	Height	m
I	Current	A
i	Current density	A m^{-2}
k	Reaction rate constant	m s^{-1}
N	Flux density	mol m^{-2} s^{-1}

n	Number of electrons	Dimensionless
$\vec{n}$	Unit outer normal	Dimensionless
p	Pressure	Pa
Q	Heat source	W m^{-3}
R	Molar gas constant	J mol^{-1} K^{-1}
S	Source/sink flux term	mol m^{-3} s^{-1}
T	Temperature	K
t	Time	s
u	X-component of velocity	m s^{-1}
$\vec{u}$	Phase velocity	m s^{-1}
V	Volume	m^3
v	Y-component of velocity	m s^{-1}
$\vec{v}$	Average velocity	m s^{-1}
w	Width	m
z	Charge number	Dimensionless

Greek

Symbol	**Definition**	**Unit**
ΔG	Change in Gibbs free energy	J mol^{-1}
ΔH	Change in enthalpy	J mol^{-1}
ΔS	Change in entropy	J mol^{-1} K^{-1}
ϕ_e	Ionic potential	V
ϕ_s	Electronic potential	V
η	Overpotential	V
λ	Thermal conductivity	W mol^{-1} K^{-1}
μ	Dynamic viscosity	Kg m^{-1} s^{-1}
ρ	Density	Kg m^{-3}
σ	Electronic conductivity	S m^{-1}
σ_e	Ionic conductivity	S m^{-1}
ζ_v	Voltage efficiency	Dimensionless
ω	Flow rate	m^3 s^{-1}

Subscripts	**Meaning**
app	Applied
e	Electrolyte property
H^+	proton property
i, j, k	Species
l	Liquid phase property
Pb^{2+}	Lead ion property
ref	Reference value
s	Solid property
0	Standard or reference value
1	Negative electrode redox reaction
2	Positive electrode redox reaction
+	Positive electrode
−	Negative electrode
Upscripts	**Meaning**
eq	Equilibrium
in	Inlet
out	Outlet
0	Initial
⟶	Vector property
—	Volume-averaged property

REFERENCES

[1] T. Nguyen and R. F. Savinell, "Flow Batteries", The Electrochemical Society, (2010) 54–56.
[2] T. Shibata, T. Kumamoto, Y. Nagaoka, K. Kawase, "Redox Flow Batteries for the Stable Supply of Renewable Energy", SEI Technical Review No.76, April (2013) 14–21.
[3] D. Pletcher and R. Wills, "A lead acid battery based on an electrolyte with soluble lead (II) - Part II", Phys Chem Chem Phys, 6 (2004) 1779–1785.
[4] H. Al-Fetlawi, "Modelling and Simulation of all-Vanadium Redox Flow Batteries", Ph.D., thesis, Faculty of Engineering and The Environment, University of Southampton, (2010).
[5] P K. Leung, "Development of A Zinc-Cerium Redox Flow Battery", Ph.D., thesis, Faculty of Engineering and The Environment, University of Southampton, (2011).
[6] C. P Zhang, S. M. Sharkh, F. C. Walsh, C. N. Zhang, J. C. Jiang, "The performance of a soluble lead-acid flow battery and its comparison to a static lead-acid battery", Energy Conversion and Management, 52 (2011) 3391–3398.
[7] J. Collins, G. Kear, X. Li, C. T. John, D. Pletcher, R. Tangirala, D. Sratton-Campbell, F. C. Walsh, C. Zhang, "A lead acid battery based on an electrolyte with soluble lead (II) - Part VII. The cycling of 10 cm × 10 cm flow cell", Journal of Power Sources, 195(2010) 1731–1738.
[8] R. G. A. Wills, J. Collins, D. Stratton-Campbell "Developments in the soluble lead-acid flow battery", Journal of Applied Electrochemistry 40 (2010) 955–965.
[9] D. Pletcher and R. Wills, "A lead acid battery based on an electrolyte with soluble lead (II) - Part III. The influence of conditions on battery performance", Journal of Power Source 149 (2005) 96–102.
[10] A. Hazza, D. Pletcher, R. Wills "A lead acid battery based on an electrolyte with soluble lead (II) - Part I. Preliminary studies", Phys Chem Chem Phys, 6 (2004) 1773–1778.
[11] H. Bode, "Lead acid batteries", John Wiley, 1977.
[12] M. Barak, P. Peregrinus, Stevenage, "Primary and secondary batteries", Electrochemical Power Sources, (1980).
[13] S. G. Bratsch, "Standard electrode potentials and temperature coefficients in water at 298.15 K", J. Phys. Chem. Ref. Data, 18 (1989) No.1, P.1–21.
[14] I. Rubenstein, "Physical Electrochemistry", Marcel Dekker, (1995).
[15] A. A. Shah, X. Li, R. G. A. Wills, F. C. Walsh, "A mathematical model for the soluble lead-acid flow battery", Journal of the Electrochemical Society, 157-A (2010) 589–599.
[16] A. Bates, S. Mukerjee, S. C. Lee, D-H. Lee, S. Park, "An analytical study of a lead-acid flow battery as an energy storage system" Journal of Power Sources, 249 (2014) 207–218.
[17] A. Bard, R. Parsons, J. Jordan, "Standard potentials in aqueous solutions", Marcel Dekker, New York, (1985).
[18] H. Al-Fetlawi, A. A. Shah, F. C. Walsh, "Non-isothermal modeling of the all-vanadium redox flow battery", Electrochimica Acta, 55 (209) 78–89.

AUTHORS BIOGRAPHY

Amir A-K Omran was born in Karbala City, Iraq, in 1990. He received the BSc in Electrochemical Engineering from the University of Babylon, Hila City, in 2012 and the MSc in Electrochemical Engineering from the University of Babylon, Hila City, in 2014.

Hassan Abdul-Zehra Abdul-Yima was born in Babylon, Iraq, in 1965. He received the BSc in Chemical Engineering from the University of Baghdad, Baghdad City, in 1988, the MSc in Chemical Engineering from the University of Baghdad, Baghdad City, in 1993, and the PhD in Electrochemical Engineering from Southampton University, United Kingdom, in 2011.